Received: 20 April 2021 | Revised: 8 June 2021 | Accepted: 7 July 2021

DOI: 10.1002/jbio.202100132

RESEARCH ARTICLE

JOURNAL OF BIOPHOTONICS

Toward optical spectroscopy-guided lung biopsy: Demonstration of tissue-type classification

Eladio Rodriguez-Diaz[1] | Samer Kaanan[2] | Christopher Vanley[2] | Tauseef Qureshi[2] | Irving J Bigio[1,3*]

[1]Department of Biomedical Engineering, Boston University, Boston, Massachusetts, USA

[2]Providence Mission Hospital, Mission Viejo, California, USA

[3]Department of Electrical & Computer Engineering, Boston University, Boston, Massachusetts, USA

***Correspondence**
Prof. Irving J Bigio, Department of Biomedical Engineering, Boston University, 44 Cummington Mall, Boston, MA 02215, USA.
Email: bigio@bu.edu

Abstract

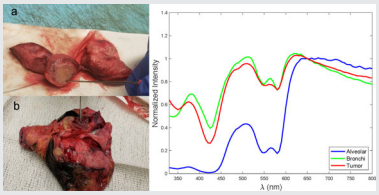

The diagnostic yield of standard tissue-sampling modalities of suspected lung cancers, whether by bronchoscopy or interventional radiology, can be non-optimal, varying with the size and location of lesions. What is needed is an insitu sensor, integrated in the biopsy tool, to objectively distinguish among tissue types in real time, not to replace biopsy with an optical diagnostic, but to verify that the sampling tool is properly located within the target lesion. We investigated the feasibility of elastic scattering spectroscopy (ESS), coupled with machine learning, to distinguish lung lesions from the various nearby tissue types, in a study with freshly-excised lung tissues from surgical resections. Optical spectra were recorded with an ESS fiberoptic probe in different areas of the resected pulmonary tissues, including benign-margin tissue sites as well as the periphery and core of the lesion. An artificial-intelligence model was used to analyze, retrospectively, 2032 measurements from excised tissues of 35 patients. With high accuracy, ESS was able to distinguish alveolar tissue from bronchi, alveolar tissue from lesions, and bronchi from lesions. This ex vivo study indicates promise for ESS fiberoptic probes to be integrated with surgical intervention tools, to improve reliability of pulmonary lesion targeting.

KEYWORDS

lung, machine learning, robotics, spectroscopy, surgical equipment

1 | INTRODUCTION

Lung cancer is the numberone cause of cancer deaths for both genders worldwide [1]. In the United States, lung cancer is diagnosed in ~230 000 patients with over 135 000 deaths annually [1]. The choice of modality for biopsy of lung lesions depends on the location and size of the lesion. Advanced bronchoscopy and radiologic biopsy techniques have been shown to be safe, with an overall high sensitivity and specificity for the diagnosis of lung cancer [2, 3]. These procedures do come with inherent risks, however. A non-encompassing list of risk factors includes infections, bleeding, pneumothorax, respiratory failure requiring life support. Moreover, in the event of an inadequate sampling or diagnosis, there can be a need for additional biopsy procedures. For central tumors, tissue biopsy is typically performed in a single session with conventional bronchoscopy, with or without

endobronchial ultrasound (EBUS) for lymph-node sampling. Central lung cancers can present as peribronchial in nature, causing extrinsic compression, which can be biopsied blind or with the aid of EBUS. Central tumors may also present as a visible exophytic lesion or submucosal spread. When combining the modalities of direct forceps biopsy, washings, brushings, and endobronchial needle aspiration techniques, the overall sensitivity of flexible bronchoscopy for diagnosing lung cancer for central endobronchial lesions is 88% [3].

Bronchoscopy with EBUS-directed biopsy has emerged as a commonly used modality for diagnosis and staging of suspected lung cancers, due to the high accuracy for both the lung lesion and for mediastinal lymphadenopathy. In one study looking at peripheral lung lesions and subsequently-diagnosed lung cancer, the sensitivity of endobronchial ultrasound-guided transbronchial needle aspiration (EBUS-TBNA) was 79% [4]. Under optimal conditions, with appropriate patient selection and adequate operator experience, the sensitivity of real-time EBUS-TBNA for establishing a diagnosis of abnormal lymph nodes in the face of suspected cancer can be up to 94% [5].

For lesions that are smaller or more peripheral, however, diagnostic yield can be adversely affected by suboptimal tool location. Biopsy options include traditional bronchoscopy, with or without EBUS, electromagnetic navigation bronchoscopy (ENB), or transthoracic needle biopsy (TTNB). The sensitivity of flexible bronchoscopy for locating peripheral lesions >2 cm is 63%, and for <2 cm in size is only 34% [3]. Thus, as lesions become more peripheral, traditional fiberoptic bronchoscopy or EBUS-TBNA are not viable options, and this is where ENB shows promise. Looking at initial 1-year results of the prospective multicenter NAVIGATE study, the 12-month diagnostic sensitivity for malignancy was 69% and specificity was 100% [6]. Even with an ENB-guided biopsy, however, up to 13.3% of biopsy samples can be read as inconclusive [7]. When bronchoscopic procedures cannot be performed, either due to technical limitations or patient safety concerns, TTNB may be an option. TTNB involves passing a percutaneous needle into lung or lymph node tissue under image guidance. In a meta-analysis comparing data from several studies up to 2004, pooled sensitivity of TTNB for the diagnosis of peripheral bronchogenic carcinoma was 90% [3].

Despite advances in the diagnosis of lung cancer, limitations remain and imperfect yield of cancer cells still results in delayed or missed diagnoses of lung cancer. Additionally, as mentioned above, these procedures do not come without known potential morbidity. While rapid onsite cytologic evaluation has helped to maximize the yield of malignant biopsies, there must be a better way to improve diagnostic yield while minimizing patient risk from each individual biopsy modality. *What is needed is a sensor-enabled technology that can objectively distinguish among tissue types in real time, without changing the work-flow or familiarity of standard surgical-intervention tools*. The primary purpose of such a technology would not be to replace traditional biopsy with a new diagnostic method, but to verify that the sampling tool is properly located within the target lesion to assure an adequate yield of cells. Here we report preliminary studies to assess the accuracy of elastic scattering spectroscopy (ESS), coupled with artificial intelligence methods for classification, for distinguishing tissue types in the lung.

Various types of optical spectroscopy for tissue classification have been described in the literature as minimally-invasive means to generate optical signatures that can identify the differences among different types of tissues and conditions, healthy and non-healthy, without the need to remove the tissue from the body [8]. The method of ESS for tissue diagnostics has been developed for over two decades as one such form of "optical biopsy" and has been demonstrated to provide good diagnostic accuracy in a number of clinical studies. Clinical studies of ESS have included: identification of metastatic involvement of breast sentinel lymph nodes during surgery [9–11]; sensing dysplasia during surveillance of Barrett's Esophagus [12]; assessment of colon polyps during a colonoscopy [13]; differentiation of normal colonic mucosa from chronic colitis and other states of inflammatory bowel disease [14]; determination of tumor margins during oral cancer surgery [15]; and distinguishing the various types of skin cancer from benign dermatological lesions [16].

Of relevance to the long-term goal of the study reported here, we have previously reported a clinical study of US-guided percutaneous sampling of thyroid nodules by fine-needle aspiration (FNA), in which an ESS probe was integrated in the lumen of the 23-gauge FNA tool [17].

Dr. Bigio's group at Boston University (extending earlier work by Bigio and Mourant) developed the method of ESS [18], and were first to demonstrate the potential benefits of clinical tissue diagnosis based on the scattering properties of cellular micromorphology [19]. ESS, as originally conceived, is a point spectroscopic measurement technique, over a broad wavelength range (320–900 nm in our current system), which, when performed using appropriate fiberoptic geometry, is sensitive to the microscopic morphological differences in tissues at the cellular and sub-cellular levels. These include nuclear size and density, hyperchromaticity, DNA condensation and chromatin granularity, nuclear crowding, and changes in the size/density of mitochondria and other cellular organelles, or structural proteins. Thus, ESS spectra derive from the wavelength-dependent optical scattering efficiency and the effects of changes in the angular

probability distribution for light scattering (the scattering "phase-function") due to the optical-index gradients of cellular and subcellular structures. Figure 1 shows the geometry of the optical measurements. With this geometry and small source-detector separation (~200 μm), the reflectance detected is sub-diffuse (rather than diffuse), resulting in high sensitivity to large-angle backscattered light, which is spectrally sensitive to variations in micromorphology and ultrastructure.

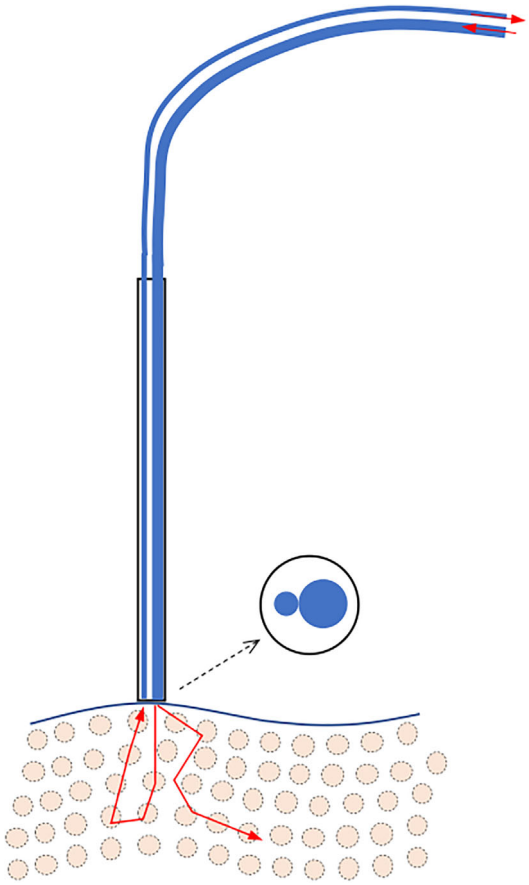

FIGURE 1 Diagram of the optical geometry for the elastic scattering spectroscopy (ESS) fiber-optic tissue measurements. A 200-μm core diameter fiber conveys light from a pulsed xenon arc lamp to the tissue surface. An adjacent fiber, with core diameter 100 μm, collects scattered light and transmits it to the spectrometer for recording and analysis. The probe tip is in contact with the tissue, avoiding specular reflection

As a result of such ultrastructural changes, normal and abnormal tissues generate different scattering spectral signatures, representing the optical-spectroscopy equivalent of histological appearances. The ESS method senses those morphology changes in a quantitative (objective) manner, without actually imaging the microscopic structure. Bigio's group and others have performed translational clinical studies (including those listed above) to ascertain the efficacy of ESS-based optical biopsy to distinguish between disease states in a variety of organ sites [20–24], some with large patient accruals [13, 22].

Earlier studies by other groups have explored various types of "optical biopsy" for detecting lung cancer and to aid in bronchoscopy or TTNB. Some of those publications reported utilizing a combination of fluorescence spectroscopy and diffuse reflectance spectroscopy (DRS) [25, 26], and other reports were focused on variations of DRS [27–29], with commendable statistics to distinguish between malignant tumors and "normal lung tissue." In comparison, our study was aimed at assessing the ability of ESS to classify and distinguish among a larger number of tissue classes: different "normal" lung tissues, as well as lesions that are distinct from normal tissues. This was to address the future feasibility to use ESS as an aide in guiding fine-needle assay to more remote pulmonary lesions, especially for "blind" robotically-guided biopsies, and to validate proper needle placement in a lesion, regardless of its pathology. Additionally, in the earlier studies, more fibers and larger source-detector separations for DRS were used (compared with our fiberoptic geometry for ESS), which required large needles of 13 to 16 gauge, whereas the fibers of our ESS geometry would fit in a 23 to 25 G fine needle [30].

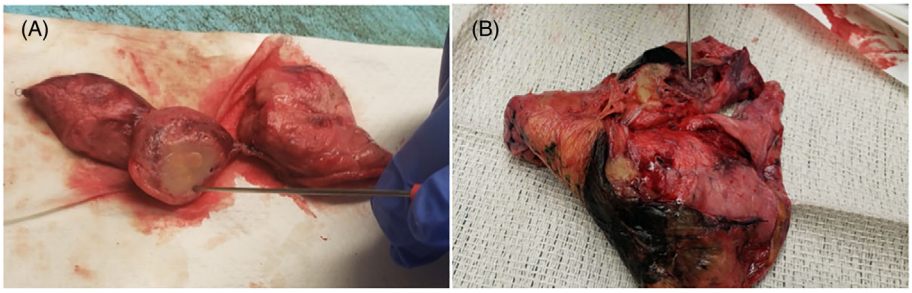

FIGURE 2 The outer tubing of the probe tool is 2.5-mm in diameter, for ease of handling with gloves, while the optical fibers are centered in the tubing with the polished fiber tips flush with the end of the probe. A, The tip of the handheld elastic scattering spectroscopy (ESS) fiberoptic probe is in contact with a bisected lesion, the measurement being made near the periphery of the lesion; B, the probe is in contact with alveolar tissue

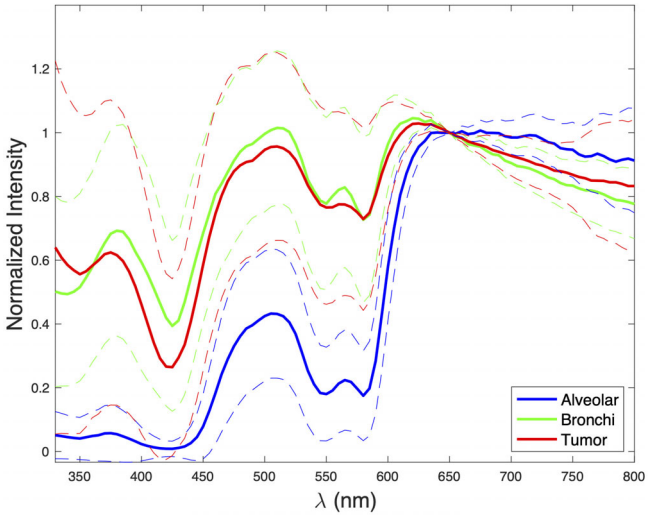

FIGURE 3 Representative elastic scattering spectroscopy (ESS) spectra of alveolar tissue, bronchi, and lesion. Standard deviations for each class are shown with dashed lines

For studies conducted in various organs, including this study, a typical ESS probe consists of two optical fibers (in this case, 100 and 200 μm), adjacent to each other. Due to the small separation of the source and detector fibers, the collected light predominantly samples a tissue volume of <0.1 mm^3. In addition, given the small source-detector separation and the consequent short average photon pathlength, in most solid tissues the method is more sensitive to scattering properties than to absorption [31]. Nonetheless, strong absorbers such as oxy- and deoxy-hemoglobin can be quantified. Specifically in this study, as can be seen in Figure 3, absorption by Hb actually dominates the spectra from alveoli, in which the air pockets exhibit much lower scattering than would be the case for solid tissue, resulting in less scattering and spectral domination by the Hb absorption. On the other hand, even though the HB absorption bands are still seen, the spectra for bronchi and tumor are differentiated by variations in the spectral shapes of the scattering component.

2 | PATIENTS AND METHODS

2.1 | Patient accrual and informed consent

The study was carried out at the Providence Mission Hospital (Mission Viejo, California), and the protocol was approved by the Mission Hospital Institutional Review Board (IRB). Only patients who were scheduled for a surgical lung resection for suspicious lesions as part of their standard of care at Mission Hospital were considered. Prior to surgery, potential subjects were contacted and informed of the objectives, procedures and possible risks/benefits of this research. The study was voluntary and was emphasized as such to potential participants, who read and confirmed understanding before signing the Informed Consent Form. Participation in the study protocol did not require alteration of a participant's surgical procedure, nor did it affect the histopathological study of the tissue specimens, the physician's decision-making or clinical management of the participants.

2.2 | Instrumentation

The ESS system used in this study consisted of a broadband pulsed xenon short-arc lamp (Hamamatsu Corporation, Bridgewater, New Jersey), a spectrometer with microcontroller board (Avantes Inc., Louisville, Colorado), power supplies, and built-in computer with custom software, housed in a clinically-friendly, compact enclosure. ESS measurements invoke short (~10 microseconds) pulses of light, with wavelength spanning from the near-ultraviolet spectral region (~320 nm) through the visible to the near-infrared spectral region (~900 nm), transmitted to the tissue via the illumination fiber. The adjacent collection fiber conveys backscattered light from the tissue to the spectrometer, with its linear detector array incorporating a fast electronic shutter. The combination of short pulses and time-gated detection reduces effects of ambient light, allowing measurements to be acquired irrespective of lighting conditions.

The ESS fiberoptic probe used in this study consists of two adjacent fibers with 200- and 100-μm cores for illumination and detection, respectively, both with a numerical aperture of 0.22 in air. The center-to-center separation between the fibers is ~200 μm. With this probe configuration, a tissue volume of ≤0.1 mm^3 is interrogated, to a depth of ~300 μm. This average sensing depth has been determined in various prior studies by our group, and others, with Monte Carlo simulations and phantoms [32, 33] and also in an animal skin model [34]. As is well-known, the average penetration depth (for this geometry) varies with wavelength, with longer (red) wavelengths exploring somewhat deeper than the short wavelengths, due to the lower scattering coefficient in the red/NIR.

Before each procedure, a white-reference measurement was recorded by shining the light from the fiberoptic probe onto the surface a spectrally-flat, diffuse-reflectance standard (Spectralon, Labsphere Inc., North Sutton, New Hampshire) and recording the reflected spectrum as a reference. This reference measurement

was used to calibrate the system response for subsequent tissue measurements, which takes into account spectral variations of the light source, spectrometer, fiber transmission and fiber coupling.

2.3 | Data collection

Freshly excised lung tissues, from patients scheduled for surgical resection as part of the standard of care, were examined in the pathology department. Spectral readings were taken on these ex vivo tissues following surgical resection. Samples were rinsed with saline to remove excessive surface blood, the tip of the fiberoptic probe was placed in gentle contact with the exposed surface at a variety of locations of tissue, and optical spectra were recorded by the ESS system (see Figure 2). Each measurement takes less than 50 ms. A variety of tissue types was sampled, including the lesions, to provide a total of 2032 spectra for comparison of the tissue types in the excised tissue. Healthy-margin tissue sites were sampled first; then the pathological sample (the lesion) was bisected, so that ESS measurements could be recorded from various locations at both the periphery and core of the lesion, mimicking a range of needle placements interstitially in the tissue. The normal tissue types for the measurements were identified by the pathologist, and histopathology reports of lesion sites were correlated with ESS spectra. After completion of the spectral measurements, the samples were transferred to pathology for standard histopathology assessment. The extra time required for the ESS measurements, a total of a few minutes, did not have any detrimental effect on the excised tissues for purposes of histopathology analysis.

2.4 | Data analysis

The recorded ESS spectra were pre-processed prior to analysis. Raw ESS spectra consisted of 1347 bands, corresponding to the pixel-density of the detector in the spectrometer, covering the wavelength range of 300 to 900 nm. Spectral bands were averaged to the nearest integer wavelength value, resulting in 601 bands in that range. Dimensionality was further reduced by smoothing and down-sampling the resulting measurements by averaging blocks of five bands and by limiting the spectral range used in subsequent analyses to the wavelength range of 330 to 800 nm. The resulting spectral measurements consisted of 95 bands. These preprocessing steps were performed to reduce high-frequency spectral noise due to pixelation and to remove the regions of the spectra with low signal-to-noise ratio arising from low detector sensitivity and lower source light intensity at the extremes of its output spectrum. Each spectrum was then normalized to the intensity at 650 nm to enable comparison based purely on spectral shape, independent of relative intensities. We have frequently used 650 nm as the normalization wavelength, since it is located in a relatively featureless region of the ESS spectra. Figure 3 shows average ESS spectra for different tissue types measured in the study. Dichotomous classifiers were designed using random forests [35]. Random forests is an ensemble classifier that trains a number of decision trees, with each tree trained on different subsets generated by randomly sampling with replacement of the training set, in conjunction with a randomly sampled subset of features. The normalized ESS spectra served as inputs to the classification models, thus in our approach these models are built based on relative changes in the measured spectra at individual wavelengths. Leave-one-patient-out (LOPO) cross-validation was used to obtain diagnostic performance estimates. This approach trains a classification model using data from all but one patient, using data from the excluded patient for testing. The process is repeated until each patient has been excluded from the training process. Unlike the commonly used leave-one-out (LOO) cross-validation, LOPO strives to reduce the bias in performance estimates caused by the correlation between measurements in the same patient.

3 | RESULTS

A total of 2032 independent ESS measurements collected from the excised tissues of 35 patients were analyzed in the study. The measurements were acquired from a variety of locations on alveolar tissue, bronchi and lesions encountered in the excised lung tissue. Lesion pathologies, confirmed by histopathology, included adenocarcinoma, carcinoid tumor, metastatic tumors, pulmonary infarction, squamous cell carcinoma (SCC) and small-cell carcinoma. Other pathologies encountered in a few lesions were scar tissue, fungal infection and inflammatory nodules. Dichotomous classifiers were built based on the pairwise combinations of the three main tissue types measured: alveolar tissue, bronchi and lesions. When training these models, no distinctions were made among the individual lesion pathologies; all lesion pathologies were treated as a single "lesion" class. Table 1 summarizes the distribution of measured ESS spectra based on tissue types and pathologies.

First, we investigated the capability of ESS to differentiate alveolar tissue from bronchi. Analysis of 437 measurements of different sites on alveolar tissues and 171 measurements of bronchi resulted in a sensitivity of 0.93, specificity of 0.91, and overall accuracy of 0.92,

TABLE 1 Breakdown of tissue types examined in the study

Tissue type	Pathology	Number of specimens	Number of spectra
Alveolar			437
Bronchi			171
Lesion/tumor			712
	Adenocarcinoma	21	349
	Carcinoid	1	17
	Fungus	1	23
	Inflammation	1	20
	Metastatic tumor	10	178
	Pulmonary infarction	1	20
	Squamous cell carcinoma (SCC)	4	87
	Scar tissue	1	6
	Small cell carcinoma	1	12

TABLE 2 Performance in distinguishing alveolar tissue from lesions

Tissue type	Pathology	Number of spectra	Performance
Alveolar		437	Specificity: 0.88
			Sensitivities:
Lesion/tumor		712	0.91
	Adenocarcinoma	349	0.89
	Carcinoid	17	0.71
	Fungus	23	1
	Inflammation	20	1
	Metastatic tumor	178	0.96
	Pulmonary infarction	20	0.85
	Squamous cell carcinoma (SCC)	87	0.91
	Scar tissue	6	0.5
	Small cell carcinoma	12	1

assuming bronchi as the positive class. Next, we assessed the performance of ESS in distinguishing alveolar tissue from lesions. We analyzed 437 measurements of alveolar tissue and 712 measurements of different lesions. This analysis resulted in a sensitivity of 0.91, specificity of 0.88, and accuracy of 0.90. A sub-analysis of these measurements based on their location showed that the specificity of alveolar tissue away from the lesion to be 0.90, with a specificity of 0.86 for alveolar tissue adjacent to lesion. Similarly, the sensitivity of lesion measurements made at the lesion core was 0.92, and the sensitivity of lesion measurements made at the periphery of lesions was 0.88. In addition, in a sub-analysis based on the individual lesion pathologies, we observed a sensitivity of 0.89 for measurements made on lesions found to be adenocarcinoma based on histopathology, a sensitivity of 0.96 for measurements of metastatic tumors, and 0.91 for SCCs. Table 2 summarizes the performance obtained when distinguishing alveolar tissue from various lesions. Finally, we examined the use of ESS to differentiate bronchi from lesions. Analyzing 171 measurements of bronchi with 712 measurements from lesions resulted in a sensitivity of 0.86, specificity of 0.82, and accuracy of 0.85. Similar performance levels were achieved, whether the measurements were made at the lesion's core, 0.86, or at the lesion's periphery, 0.85. Table 3 shows the performance achieved in differentiating bronchi from lesions, including results for sub-analysis of different types of lesion pathologies. The sensitivity was found to be 0.83 in adenocarcinomas, 0.93 in metastatic tumors, and 0.89 in SCCs.

TABLE 3 Performance in distinguishing bronchi from lesions

Tissue type	Pathology	Number of spectra	Performance
Bronchi		171	Specificity: 0.83
			Sensitivities:
Lesion/tumor		712	0.86
	Adenocarcinoma	349	0.83
	Carcinoid	17	0.71
	Fungus	23	0.61
	Inflammation	20	0.95
	Metastatic tumor	178	0.93
	Pulmonary infarction	20	0.95
	Squamous cell carcinoma (SCC)	87	0.89
	Scar tissue	6	0.67
	Small cell carcinoma	12	0.83

4 | COMMENT

More people die of lung cancer than any other form of cancer, and it is acknowledged that earlier identification and treatment of small lesions (including hard-to-target distal lesions) would help for extension of life expectancy. One of the challenges, however, to the proper identification and treatment of peripheral lesions (and involved lymph nodes) relates to a significant percentage of misses in directing the sampling tool into the suspect lesion, following "blind" guidance of the tool to the lesion, even with electromagnetic navigation or radiological imaging. Thus, in the rapidly evolving areas of robotically-enabled interventional radiology, electro-magnetically guided robotic or manual bronchoscopy and traditional percutaneous needle interventions, there is great potential benefit from sensor-integrated surgical tools that provide real-time identification of tissue types at the tip of the tool. Given the potential for ESS fiberoptic probes to be very small, fitting within, say, a 23-gauge (0.6 mm OD) or smaller needle, we sought to explore the potential for ESS to instantaneously identify tissue types in the lung, with the goal of demonstrating the promise for future development of image-guided robotic and traditional biopsy tools that integrate ESS fiberoptic probes. This is a platform technology, with a myriad of potential applications in other guided-biopsy tissue sites, and in this study, we begin with the typing of lung tissues, motivated by the large disease numbers and the potential impact of any improvement in diagnostic accuracy.

Existing image-guided interventions, either manual or robotically enabled, exhibit target-accuracy limitations. Tools that are tracked manually, electro-magnetically or with optical guidance, are registered over a live or saved image (MRI/CT/Xray/Ultrasound or video); but there is no direct feedback mechanism indicating that the tip of the tool is actually in the targeted tissue. The tool location is estimated computationally and displayed to the user in virtual maps. The ESS platform allows any surgical tool, whether manually or robotically guided, to provide real-time feedback to confirm targeted tissue type. The benefits of such feedback would be especially valuable when diagnostic cell-yield is problematic under current practice, or in locations where there may be risk of injury to, say, critical nerves or blood vessels. Given the clinically-friendly fundamental design of ESS-based tissue classification, mediated by fine fiberoptic probes, it will be possible to integrate the technology cost-effectively into various surgical-intervention devices, including tissue-sampling tools. In the management of lung cancer, those tools include the range of advanced bronchoscopy tools and specialized percutaneous needles designed for interventional-radiology methods.

4.1 | Limitations

The modest number of patients in this preliminary study limited the statistical analysis to a retrospective estimate of classifier performance, which is classically optimistic. In a larger study, separate training and testing sets would be used to more reliably assess prospective accuracy. Nonetheless, despite the fact that prospective studies are typically less optimistic than retrospective analysis, a larger dataset would also enable training of more-sophisticated classification algorithms, potentially leading to even higher diagnostic accuracies. Another limitation is that these preliminary studies were based on

measurements in ex-vivo tissue samples, lacking active perfusion. Still, since the ESS spectral signatures are based more on the scattering (hence, microstructural) properties of the tissue, and less on the hemodynamic properties, differences between ex-vivo and in-vivo measurements are typically modest, and ex-vivo data can be predictive of clinical translational potential.

In summary, we have presented ESS as a viable platform for differentiating tissue types in the lung. Going forward, we plan to develop a needle-lumen ESS probe, which can be inserted through the needle during an image-guided percutaneous (transthoracic) lung biopsy. ESS spectra will be compared with the resulting histopathology reports of the correlated tissue samples to assess the potential for reducing the incidence of nondiagnostic yield in real-world clinical use. The fact that small fiberoptic probes can readily be interfaced with tissue-samplings tools, and that ESS has the potential to accurately discriminate different tissue types in the lung, makes ESS a promising technology for improved reliability of biopsy and tissue targeting.

ACKNOWLEDGMENTS

The authors thank Boston University (Office of Technology Development) for the loan of the ESS instrument and probe for these studies. The authors also thank the staff at Mission Hospital in the operating room, pathology department and IRB for their support, professionalism, and dedication to better patient outcomes.

DISCLOSURE OF INTEREST

ERD and IJB disclose equity positions in Concur Biophotonics, LLC. While the results of this study are of interest to Concur, the company did not provide any funding for the reported work, nor was any compensation provided to any of the participants. Moreover, the company did not have any oversight of what is published here.

DATA AVAILABILITY STATEMENT

Research data are not shared.

ORCID

Eladio Rodriguez-Diaz https://orcid.org/0000-0001-7750-9110

REFERENCES

[1] R. L. Siegel, K. D. Miller, A. Jemal, *CA. Cancer J. Clin.* **2020**, *70*(1), 7.

[2] A. R. Belanger, J. A. Akulian, *Therapeutic Advances in Respiratory Disease* **2017**, *11*, 211.

[3] M. P. Rivera, A. C. Mehta, M. M. Wahidi, *Chest* **2013**, *143*(5), e1425.

[4] G. Paone, E. Nicastri, G. Lucantoni, R. Della Iacono, P. Battistoni, A. L. D'Angeli, G. Galluccio, *Chest* **2005**, *128*(5), 3551.

[5] F. J. F. Herth, R. Eberhardt, P. Vilmann, M. Krasnik, A. Ernst, *Thorax* **2006**, *61*, 795.

[6] E. E. Folch, M. A. Pritchett, M. A. Nead, M. R. Bowling, S. D. Murgu, W. S. Krimsky, B. A. Murillo, G. P. LeMense, D. J. Minnich, S. Bansal, B. Q. Ellis, A. K. Mahajan, T. R. Gildea, R. I. Bechara, E. Sztejman, J. Flandes, O. B. Rickman, S. Benzaquen, D. K. Hogarth, P. A. Linden, M. M. Wahidi, J. S. Mattingley, K. L. Hood, H. Lin, J. J. Wolvers, S. J. Khandhar, C. Anciano, A. Aragaki, D. Arenberg, O. Awais, R. Balestra, E. Barisione, R. Bechara, M. Bezzi, K. Bhadra, J. Bird, A. Blanco, M. Bowling, R. Cerfolio, M. Christensen, J. Cicenia, A. Courey, J. Doty, K. Eggleston, B. Ellis, I. Fernandez, E. Folch, A. Furman, G. D. Gass, T. Gildea, A. Gogineni, M. F. Grabcanovic, J. D. Hinze, D. K. Hogarth, R. Karunakara, J. Kazakov, S. Khandhar, S. Khurana, W. Krimsky, G. Krishna, R. Krol, R. Kropfmüller, B. Lamprecht, K. Lau, A. Lee, G. LeMense, P. Linden, P. Lutz, A. Mahajan, K. Mahmood, F. Maldonado, R. Martinez, J. Mattingley, D. Minnich, S. Murgu, B. Murillo, K. Nason, M. Nead, C. Parks, K. Perret, P. Porsch, M. Pritchett, O. Rickman, M. Rosario, M. Salio, S. Sarkar, A. Seevaratnam, S. Sethi, J. Singh, M. Studnicka, T. Takubo, C. Teba, C. Towe, M. Trigiani, J. R. Vergnon, N. E. Viby, M. Wahidi, E. Waller, B. Wei, D. Zanchi, M. Zgoda, *J. Thorac. Oncol.* **2019**, *14*(3), 445.

[7] S. J. Khandhar, M. R. Bowling, J. Flandes, T. R. Gildea, K. L. Hood, W. S. Krimsky, D. J. Minnich, S. D. Murgu, M. Pritchett, E. M. Toloza, M. M. Wahidi, J. J. Wolvers, E. E. Folch, *BMC Pulm. Med.* **2017**, *17*, 59.

[8] I. J. Bigio, J. R. Mourant, *Phys. Med. Biol.* **1997**, *42*, 803.

[9] K. S. Johnson, D. W. Chicken, D. C. O. Pickard, A. C. Lee, G. Briggs, M. Falzon, I. J. Bigio, M. R. Keshtgar, S. G. Bown, *J. Biomed. Opt.* **2004**, *9*, 1122.

[10] M. R. S. Keshtgar, D. W. Chicken, M. R. Austwick, S. K. Somasundaram, C. A. Mosse, Y. Zhu, I. J. Bigio, S. G. Bown, *Br. J. Surg.* **2010**, *97*, 1232.

[11] Y. Zhu, T. Fearn, D. W. Chicken, M. R. Austwick, S. K. Somasundaram, C. A. Mosse, B. Clark, I. J. Bigio, M. R. S. Keshtgar, S. G. Bown, *J. Biomed. Opt.* **2018**, *23*, 1.

[12] Y. Zhu, T. Fearn, G. MacKenzie, B. Clark, J. M. Dunn, I. J. Bigio, S. G. Bown, L. B. Lovat, *J. Biomed. Opt.* **2009**, *14*, 1.

[13] E. Rodriguez-Diaz, Q. Huang, S. R. Cerda, M. J. O'Brien, I. J. Bigio, S. K. Singh, *Gastrointest. Endosc.* **2015**, *81*, 539.

[14] E. Rodriguez-Diaz, C. Atkinson, L. I. Jepeal, A. Berg, C. S. Huang, S. R. Cerda, M. J. O'Brien, I. J. Bigio, F. A. Farraye, S. K. Singh, *Inflamm. Bowel Dis.* **2014**, *20*(6), 1029.

[15] G. A. Grillone, Z. Wang, G. P. Krisciunas, A. C. Tsai, V. R. Kannabiran, R. W. Pistey, Q. Zhao, E. Rodriguez-Diaz, O. M. A'Amar, I. J. Bigio, *Laryngoscope* **2017**, *127*, S1.

[16] E. Rodriguez-Diaz, D. Manolakos, H. Christman, M. A. Bonning, J. K. Geisse, O. M. A'Amar, D. J. Leffell, I. J. Bigio, *Photochem. Photobiol.* **2019**, *95*(6), 1441.

[17] J. C. Briggs, O. A'amar, I. Bigio, J. E. Rosen, S. L. Lee, A. Sharon, A. F. Sauer-Budge, *J. Med. Device.* **2014**, *8*, 021003.

[18] J. R. Mourant, T. Fuselier, J. Boyer, T. M. Johnson, I. J. Bigio, *Appl. Opt.* **1997**, *36*(4), 949.

[19] J. R. Mourant, I. J. Bigio, J. Boyer, T. M. Johnson, J. A. Lacey, A. G. Bohorfoush, M. Mellow, *J. Biomed. Opt.* **1996**, *1*, 192.
[20] I. J. Bigio, S. G. Bown, G. Briggs, C. Kelley, S. Lakhani, D. Pickard, P. M. Ripley, I. G. Rose, C. Saunders, *J. Biomed. Opt.* **2000**, *5*(2), 221.
[21] K. S. Johnson, D. C. O. Pickard, A. C. Lee, I. J. Bigio, M. R. Keshtgar, S. G. Bown, D. W. Chicken, G. Briggs, M. Falzon, *J. Biomed. Opt.* **2004**, *9*(6), 1122.
[22] L. B. Lovat, K. Johnson, G. D. Mackenzie, B. R. Clark, M. R. Novelli, S. Davies, M. O'Donovan, C. Selvasekar, S. M. Thorpe, D. Pickard, R. Fitzgerald, T. Fearn, I. Bigio, S. G. Bown, *Gut* **2006**, *55*(8), 1078.
[23] O. M. A'Amar, L. Liou, E. Rodriguez-Diaz, A. De Las Morenas, I. J. Bigio, *Lasers Med. Sci.* **2013**, *28*(5), 1323.
[24] O. M. A'Amar, R. D. Ley, I. J. Bigio, *J. Biomed. Opt.* **2004**, *9*(6), 1320.
[25] M. P. L. Bard, A. Amelink, M. Skurichina, V. N. Hegt, R. P. W. Duin, H. J. C. M. Sterenborg, H. C. Hoogsteden, J. G. J. V. Aerts, *Chest* **2006**, *129*, 995.
[26] J. W. Spliethoff, D. J. Evers, H. M. Klomp, J. W. van Sandick, M. W. Wouters, R. Nachabe, G. W. Lucassen, B. H. W. Hendriks, J. Wesseling, T. J. M. Ruers, *Lung Cancer* **2013**, *80*, 165.
[27] J. W. Spliethoff, W. Prevoo, M. A. J. Meier, J. De Jong, H. M. Klomp, D. J. Evers, H. J. C. M. Sterenborg, G. W. Lucassen, B. H. W. Hendriks, T. J. M. Ruers, *Clin. Cancer Res.* **2016**, *22*, 357.
[28] J. W. Spliethoff, L. L. de Boer, M. A. J. Meier, W. Prevoo, J. de Jong, T. M. Bydlon, H. J. C. M. Sterenborg, J. A. Burgers, B. H. W. Hendriks, T. J. M. Ruers, *Lung Cancer* **2016**, *98*, 62.
[29] D. J. Evers, R. Nachabé, H. M. Klomp, J. W. Van Sandick, M. W. Wouters, G. W. Lucassen, B. H. W. Hendriks, J. Wesseling, T. J. M. Ruers, *Clin. Lung Cancer* **2012**, *13*, 424.
[30] J. C. Briggs, O. A'amar, I. Bigio, J. E. Rosen, S. L. Lee, A. Sharon, A. F. Sauer-Budge, *J. Med. Devices, Trans. ASME* **2014**, *8*, 1.
[31] J. R. Mourant, A. H. Hielscher, A. A. Eick, T. M. Johnson, J. P. Freyer, *Cancer* **1998**, *84*(6), 366.
[32] R. Reif, O. A'Amar, I. J. Bigio, *Appl. Opt.* **2007**, *46*, 7317.
[33] A. Amelink, H. J. Sterenborg, *Appl. Opt.* **2004**, *43*(15), 3048.
[34] K. Calabro, A. Curtis, J.-R. Galarneau, T. Krucker, I. J. Bigio, *J. Biomed. Opt.* **2011**, *16*, 011008.
[35] L. Breiman, *Mach. Learn.* **2001**, *45*(1), 5.

How to cite this article: E. Rodriguez-Diaz, S. Kaanan, C. Vanley, T. Qureshi, I. J. Bigio, *J. Biophotonics* **2021**, *14*(10), e202100132. https://doi.org/10.1002/jbio.202100132